Enhancement and depletion of lower/middle tropospheric ozone in Senegal during pre-monsoon and monsoon periods of summer 2008: Observations and Model results.

Gregory S. Jenkins[1], Seydi Ndiaye[2], Moussa Gueye[2], Rachel Fitzhugh[3*], Jonathan W. Smith[1], Abou Kebe[4]

1. Howard University Program in Atmospheric Science, Washington DC 20059
2. Lab for Atmospheric-Oceanic Physics-Simeon Fongang, Cheikh Anta Diop University, Dakar Senegal
3. Department of Atmospheric Ocean and Space Science, University of Michigan, Ann Arbor, Michigan. *Now at ITT Corporation 1447 St. Paul Rochester, NY 14621
4. Senegal Meteorological Agency, Dakar Senegal

Abstract

During the summer (8 June through 3 September) of 2008, nine (9) ozonesondes are launched from Dakar, Senegal (14.75°N, 17.49°W) to investigate ozone (O_3) variability in the lower/middle troposphere during the pre-monsoon through monsoon period. Results during June (pre-monsoon period) show a reduction in O_3, especially in the 850-700 hPa layer with SAL events. However, O_3 concentrations are increased in the 950-900 hPa layer where the peak of the inversion is found and presumably the highest dust concentrations. We use the WRF-CHEM model to explore the observations of elevated/reduced O_3 concentrations during the pre-monsoon/monsoon periods. In the transition period between 26 June and 2 July lower tropospheric (925-600 hPa) O_3 concentrations are likely enhanced by enhanced biogenic NO_X emissions from the Saharan desert and Sahelian soils following several rain events on 28 June and 1 July. During July and August (monsoon period), with the exception of one SAL outbreak, vertical profiles of O_3 are well mixed with concentrations not exceeding 55 ppb between the surface and 550 hPa.

1. Introduction

Understanding tropospheric ozone (O_3) variability in the tropics remains an active area of research with biomass burning, biogenic, anthropogenic and lightning being important sources of ozone production in the tropics and deposition and heterogeneous chemistry being important sink of O_3 in the tropics. Tropospheric O_3 is also a greenhouse gas with positive radiative forcing and contributes to global warming. A likely source of Northern Hemisphere summer season tropospheric O_3 variability is associated with Saharan dust events. Each year, between May and October, the Saharan Air Layer (SAL) (Carlson and Prospero, 1972; Dunion and Veldon, 2004) is a dominant feature influencing continental areas of West Africa and the Tropical Atlantic. The SAL is characterized by dry, (low relative humidity), stable air (an inversion capped above the marine boundary layer), a mid-level easterly jet and reduced visibilities from enhanced dust. Potential sources of dust are found in Mauritania, Mali and Algeria during June-July and August in association with the SAL (Middleton and Goudie, 2001).

A number of observational studies have shown reduced O_3 in the presence of Saharan dust (De Reus et al. 2000; Bonasoni et al. 2004). The desert aerosols can reduce tropospheric O_3 concentrations at a single location in multiple ways: (a) dust aerosols may serve as deposition sites for O_3 while also reducing photolysis rates. (b) Heterogeneous chemistry on aerosol surfaces can reduce important precursors (OH, HO_2) associated with O_3 production. (c) The production of Nitric Acid (HNO_3), leading to particulate nitrate can act as a sink for NO_X and limit O_3 production (Zhang et al. 1994; Jacob, 2000; Bian and Zender 2003; De Reus et al. 2000; Tang et al. 2003). Hence, the

SAL acts as a potential sink for O_3, reducing its greenhouse forcing while also scattering solar radiation causing daytime cooling at the surface.

Recent observations of the SAL have examined its radiative impact (Myhre et al, 2003), chemical composition (Twohy et al. 2008), aerosol and water vapor structure (Ismail et al. 2010), and potential impact on African Easterly Waves (AEWs) and Tropical Cyclogenesis (Jenkins et al. 2008; Zipser et al. 2009). Here we report on the variability of lower/middle tropospheric O_3 (surface through 550 hPa) during the pre-monsoon and monsoon periods of 2008 at a location in the semi-arid Sahelian zone.

2. Observational data and Model Simulations

In preparation for ozonesonde launches Vaisala ECC6AB ozonesondes were prepared 3-7 days in advance and launched in concert with RS92 radiosonde at 1200 UTC during June, July and August of 2008. Table 1 shows the 9 ozonesonde launches from Dakar, Senegal (14.75°N, 17.49°W) during the period. Aerosol observations are derived from the Aerosol Optical Thickness (AOT) measurements from the Aerosol Robotic Network (AERONET) at Mbour, Senegal (14.39°N, 16.59°W) and from the Space-borne Ozone Monitoring Instrument (OMI) Aerosol Index (AI) for the summer of 2008. The 1 ° x 1° Deep Blue product from the Moderate Resolution Imaging Spectrometer (MODIS) instrument aboard the AQUA satellite is used for AOT over land areas. Daily averages of AOT are constructed from the hourly AOT data from Mbour, Senegal. Tropospheric Column Ozone (TCO) estimates for the summer of 2008 at 1° x 1.25° are also used (Ziemke et al. 2006.)

To address daily and seasonal tropospheric O_3 variations for comparision with the

79 measurements the Weather and Research Forecasting with Chemistry (WRF-CHEM)
80 model is used to simulate O_3 concentrations over West Africa during the summer of 2008
81 (Grell et al. 2005). The WRF-CHEM computes gas phase chemistry with 55 prognostic
82 species and 134 reactions (Fast et al. 2005). The WRF-CHEM simulations use 30 km grid
83 spacing, 27 vertical levels and the top of the model is 50 hPa. The biogenic sources of
84 volatile organic compounds are computed (Guenther et al. 1995) and the model is
85 initialized from a uniform state with O_3 concentrations that increases with height to the
86 stratosphere. NCEP final analyses at 6-hour intervals provide meteorological initial and
87 boundary conditions to the WRF-CHEM. Here we define the pre-monsoon period as the
88 month of June and the monsoon period from July through September.
89
90 **3. Results**
91 Figures 1a-d show the satellite derived TCO values across West Africa and the
92 Eastern Atlantic for June through September 2008. A north-south gradient of TCO
93 values with higher TCO values are generally found over the Sahara relative to Sahelian
94 and Guinean regions of West Africa. The TCO gradient is weakest and strongest during
95 June and August respectively. During June, TCO values of 37-40 DU are found over the
96 desert regions with slightly lower values to the south (Figure 1a). However, by August
97 TCO values are considerably lower over the Sahelian and Guinea regions of West Africa.
98 Figures 2a-c show the OMI AI along with the AOT from Mbour, Senegal for the period
99 of ozonesonde launches during 2008. There are a number of high AI/AOT days
100 associated with SAL outbreaks during June and July and considerably fewer days in
101 August. The numbers of days where AI was greater than 2.5 during June, July and
102 August were five (5), three (3) and one (1) respectively. The numbers of days where

AOT values are greater than 0.6 during June, July and August are seven (7), four (4) and two (2), respectively. The OMI AI is positive correlated to the Mbour AOT values with correlation values of 0.82, 0.86 and 0.79 during June, July and August respectively. TRMM daily averaged rain amounts for a 5° ×5° (11.5-16.5°N, 12.5-17.5°W) box over Senegal and Gambia shows very little precipitation until the end of June when wetter conditions begin and continue through July and August (Figure 2d).

Figure 3a shows ozonesondes for the summer of 2008 with a range in O_3 concentrations from approximately 20-80 ppb between the surface and 450 hPa. Table 1 shows that highest column ozone in the 925-550 hPa layer is found on 12 June (20.5 DU) with 14.2 DU on 2 July. The lowest column ozone in the 925-550 hPa layer is found on 27 September (6.4 DU) followed by 8 June (6.6 DU). Figure 3b shows the two vertical profiles of O_3 between the end pre-monsoon period and the start of the monsoon season; a significant enhancement is found between the surface and 600 hPa. We discuss possible causes for elevated O_3 during the transition period in Section 3.2.

3.1 Pre-monsoon O_3 measurements

There are three (3) ozonesonde launches, 8, 10, 15 June with OMI AI values > 2 which are associated with SAL events in Figure 2. During the pre-monsoon period (Figure 4a), O_3 concentrations are reduced on 8 and 10 June relative to the other profiles, especially in the 850-600 hPa layer. These are also the two days with the lowest 925-550 hPa column ozone during the pre-monsoon period (Table 1). In the 950-900 hPa layer, just below the depleted layer there is also evidence of enhanced O_3 concentrations. Figure 4b shows low relative humidity (< 20%) at approximately 950 hPa for 8, 10, 12 and 15

June, which begins to increase at pressure levels less than 700 hPa, except for 12 June where RH values rapidly increase above 900 hPa. Figure 4c shows a temperature inversion is present for all pre-monsoon ozone profiles, but the very strongest temperature inversions are found for 8, 10 and 15 June. It is at the peak of temperature inversion that increases in O_3 concentrations are found (Figure 4a). This is also the altitude where high dust concentrations are found (Ismail et al. 2010).

Figures 5a-h show OMI- AI with 925 hPa streamlines along with the Deep Blue AOT overlain by 700 hPa streamlines for comparison during the pre-monsoon period. Elevated aerosol loadings on 8, 10 and 15 June are associated with either northerly or northeasterly winds at 925 hPa (Figures 5 a, b, d). In contrast, winds with a southerly component are found on 12 June and 26 June (Figures 5c, 5e). Moreover an African Easterly Wave (AEW) (Burpee et al. 1972) at 700 hPa streamlines, exits the continent on 12 June and is associated elevated RH, cloudiness and precipitation in Dakar. Reduced O_3 concentrations between 850 and 600 hPa on 8, 10 June in concert with higher AI/AOT from Saharan dust support depletion through heterogeneous chemistry.

3.2 Pre-Monsoon/Monsoon Transition

Satellite and aircraft observations along with modeling studies have identified NO_X emissions from soil as an important source of tropospheric NO_X during June, July and August in Sahelian and Saharan zones (Jeagle et al. 2004; Van der A et al. 2008; Williams et al 2009; Delon et al. 2008; Delon et al. 2010). Pulses of biogenic NO_X emissions are released into the atmosphere from the soil at the end of the dry season with the first rains. During the 2006 African Monsoon Multidisciplinary Analyses (AMMA)

147 campaign (Redelsperger et al. 2006), aircraft measurements flown over wet/dry soils
148 during the AMMA field campaign show higher NO_X concentrations in the boundary layer
149 over the recently wet soils (Stewart et al. 2008). O_3 concentrations are significantly
150 higher over wet soils when compared to dry surfaces and low correlations with CO imply
151 that NO_X production is not associated with anthropogenic or biomass burning sources
152 (Stewart et al. 2008). A sharp gradient in O_3 concentrations are found implying produced
153 locally O_3 estimated at 1 ppb h^{-1} from soil NO_X.

154 Figure 3b shows that O_3 concentrations between 950 and 600 hPa are considerably
155 higher at the start of the monsoon period (2 July) when compared to the end of the pre-
156 monsoon period (26 June). O_3 concentrations are more than 10-20 ppb larger on 2 July
157 when compared to 26 June. The enhancement of O_3 coincides with several rainfall
158 events in Senegal that the vicinity of Dakar on 28, 30 June (Figures 6 a,b). TRMM daily
159 rain estimates were highest on 1 July with daily amount approaching 80 mm in some
160 areas to the east of Dakar (Figure 6d). The rainfall was associated with the passage of an
161 AEW on 1 July and a plausible cause for O_3 enhancement between 26 June and 2 July by
162 biogenic NO_X emissions from wet Sahelian soils.

163 *3.3 Monsoon O_3 measurements*

164 During the monsoon period, the vertical profiles of O_3 are nearly uniform on 2 July,
165 27 August and 3 September, except for 2 August when there is a SAL event affecting
166 Senegal (Figure 7a). The 2 August measurement shows the enhance/depletion pattern of
167 O_3 concentrations in the vertical profile as in earlier SAL events with enhancement near
168 the peak of the SAL temperature inversion and depletion immediately above this level.
169 Figure 7b shows humid conditions over Senegal during July, August and September

except for 2 August when a SAL event occurred over Senegal. The 2 August vertical profile of relative humidity shows values less than 10% in the 950-900 hPa layer. In contrast a very moist profile can be found on 27 August with RH values between 90 and 100% from 950 through 750 hPa. A large temperature inversion is found on 2 August in association with the SAL event with smaller temperature inversions found during the other three monsoon launches (Figure 7c). Table 1 shows that during the monsoon period the lowest column O_3 is found on 27 August in association with the highest relative humidity in the 925-550 hPa layer.

Figures 8a-h show OMI- AI with 925 hPa streamlines along with the Deep Blue AOT overlain by 700 hPa streamlines for comparison during the monsoon period. During this period, only 2 August shows elevated AI and AOT in association with a thermal low (heat low) over Southern Mauritania (Figure 8b). During the other three days (2 July, 27 August, 3 September), the highest AI or AOT values are found over higher latitudes (> 20 degrees). Also evident at 700 hPa are strong AEWs, which have closed vortices on 2 July, 27 August and 3 September (Figure 8a, c, d).

3.4 WRF-CHEM simulations of elevated O_3 concentrations on 12 June and reduced O_3 concentrations during the monsoon period.

Table 1 shows that during the period of 10 June through 12 June, the 925-550 hPa column O_3 is increased by a factor of 2.77; between the SAL air mass and the passage of the AEW. This is followed by a decreased by nearly a factor of 1.8 between 12 and 15 June. The elevated O_3 concentration on 12 June could be due to: (a) a stratospheric intrusion; (b) a biogenic pulse of NO_X from Sahelian soils enhancing O_3 or; (c) lightning-

192 NO_X which enhances O_3 concentrations that is then transported to the lower/middle
193 troposphere (Grant et al. 2008). To address a possible stratospheric influence, the WRF-
194 CHEM is initialized at four different times at 0000 UTC, 1 June; 1200 UTC, 4 June; 1200
195 UTC 5 June; 1200 UTC 6 June to simulate elevated O_3 concentration for the period 10-12
196 June.. Figures 9 a-d show for the period of 8 June and 13 June that higher concentrations
197 of O_3 are found in the middle and upper troposphere based on vertical profiles of O_3 at
198 14.5 °N, 17.5° W near Dakar, Senegal, in a region of weak sinking motion. WRF-
199 CHEM forecasts that are initialized on 5 and 6 June show O_3 concentrations in the 90 to
200 120 ppb range at the 200-300 hPa levels with values of 35-50 ppb extending downward
201 into middle to lower troposphere (Figures 9c, d).

202 The elevated levels are consistent with the observations between 10 and 12 June
203 where a large increase is found in the lower/middle troposphere (Figures 4a). For
204 example, O_3 values of 20 ppb are found near 600 hPa on 10 June but increase to nearly
205 65 ppb on 12 June. Figure 10 provides further support for a stratospheric intrusion when
206 comparing O_3 concentrations on 10, 12 June for 1000-150 hPa levels. On 12 June O_3
207 values greater than 400 ppb are found just below 200 hPa. The enhancement of O_3
208 relative to 10 June is found throughout the lower, middle and upper troposphere. Hence,
209 O_3 elevated concentrations from the lower stratospheric is supported by observations and
210 WRF-CHEM results during the period of 10-12 June.

211 Next we use WRF-CHEM to explore the lower O_3 concentrations that are
212 relatively well mixed during August and September. Table 1 shows low 925-550 hPa
213 column O_3 under moist and low aerosol loading conditions. In particular, 27 August and 3
214 September measurements show low concentrations of O_3 that are well mixed relative to

215 the O_3 measurements under humid conditions (Figure 7a). There are several factors that
216 could lead to well mixed, reduced O_3 concentrations in the monsoon season: (a)
217 increased O_3 and NO_X deposition; and (b) the northward transport of O_3 poor air from
218 areas to the south of the Sahel.

219 First, a reduction in O_3 concentrations during the monsoon period is expected
220 because of increased deposition with the rapid growth of vegetation. After June, the
221 northward movement of the monsoon and the accompanied southwest moist flow leads to
222 increased instability and precipitation. The precipitation supplies an important source of
223 moisture for vegetation growth of West Africa (Guinea region northward to the Sahel).
224 The expansion of vegetation leads to increased deposition and a north-south gradient in
225 deposition rates and hence ozone in the lower troposphere. Measurements in Senegal
226 during 2006 estimate a maximum deposition velocity of 1.5 cm-s^{-1} with higher values
227 noted during precipitation events (Grant et al. 2008). The removal of NO_X through
228 dry/wet deposition would lead to reduced O_3 concentrations in lower latitudes relative to
229 the drier semi-arid and arid regions in the Sahelian zone and Sahara desert (Delon et al.
230 2010).

231 Second, northward surges in the monsoon flow or the passage of AEWs should lead
232 to an overall poleward transport of O_3 poor air in the lower troposphere, because of more
233 vegetation and higher deposition rates in lower latitudes; onshore flow from the Atlantic
234 ocean would also transport in O_3 poor air. Conversely surges of dry air from desert
235 regions should lead an equatorward transport of enriched O_3 concentrations to lower
236 latitudes. An example of this process is the low O_3 concentrations in the lower
237 troposphere measured at Dakar, Senegal for 27 August, and 3 September. In each case,

very moist conditions with 925 hPa flow coming from Atlantic Ocean (Figure 8c) and lower latitudes (Figure 8d) are found with the approach or passage of an AEW (Figures 8g, h) at 700 hPa. AEWs on 2 July and 27 August are associated with Tropical Cyclones Bertha and Ike, respectively (Rhome 2008; Berg 2008). The monthly averaged TCO values (Figure 1) along with recent measurements during the AMMA field campaign support a north-south gradient in the lower troposphere with lower O_3 concentrations found in equatorward latitudes of West Africa (Saunois et al. 2008).

To examine simulated seasonal O_3 concentrations and its relationship to relative humidity we show WRF-CHEM forecasted 925 hPa 12-hour instantaneous O_3 concentrations and relative humidity averaged over the area of 14-16° and 18-16°W for June, July and August and early September (Figure 11). The highest O_3 concentrations are found during the month of June with significant reductions simulated during the months of July and August. Simulated O_3 concentrations of 10-20 ppb are common at 925 hPa during the monsoon period (Figure 11a) relative to June. The lower simulated O_3 concentrations are found when the simulated relative humidity (RH) at 850 hPa values begins to increase (Figure 11b). Elevated 850 hPa relative humidity can be used as a proxy of the monsoon flow during July, August and September. The simulated increases in relative humidity are in agreement with satellite observed wetter conditions during July and August (Figure 2d)

4. Discussion and Summary

During the pre-monsoon period reductions of O_3 concentrations in the lower troposphere associated with SAL outbreaks. Figures 12 a-d show the vertical profiles of O_3 concentration, relative humidity and temperature in the 1000-750 hPa layer for the four SAL events that occurred during the summer of 2008. Similar vertical profiles of O_3 concentrations (> 50 ppb for 2 August) are found in three of the four ozonesondes: An increase in O_3 concentrations is found to overlap with a temperature inversion and very low relative humidity (Figures 12a, b, d). Above the layer where O_3 concentrations are enhanced, there is a depleted layer of O_3 in the 900-750 hPa layer. The depleted O_3 layer is Figure 12 is consistent with the earlier results of De Reus et al. (2000) and Bonasoni et al. (2004) with heterogeneous chemistry being a primary source of O_3 depletion (Zhang et al. 1994; Tang et al. 2004). Tang et al. (2004) show through modeling studies and aircraft observations that losses of O_3 and HNO_3 through direct interaction with dust were large during observed dust storms in the ACE-Asia field campaign.

Figure 13a depicts the changes in aerosol concentrations, relative humidity and O_3 concentrations, during a ideal SAL events with significant dust loading, based on the findings from this study. During this SAL event, a vertical profile of O_3 would show: Layer A – from the surface to 950 hPa with slowly increasing O_3 concentrations and low aerosol concentrations; Layer B- a 50-100 hPa layer with elevated O_3, high aerosols concentrations and a strong temperature inversion; Layer C - a 100-200 hPa layer with reduced O_3 concentrations and smaller sized aerosols. One might expect the largest losses of O_3 in layer B in association with heterogeneous reactions but the observations show

283 that this is not observed and hence there must be a source of O_3. The most likely source
284 would be biogenic sources of NO_X from Saharan soils that have been lifted that act as a
285 source of atmospheric O_3 in downstream regions. The exact mechanism for O_3
286 enrichment by Saharan dust remains uncertain.

287 A suggested mechanism for enhancing O_3 concentrations in this shallow layer
288 may come from the activation of a biogenic NO_X pulse when encountering moist
289 conditions (Figure 13b). Nitrate formation on dust aerosols is an end-product after
290 heterogeneous reactions between HNO_3 and dust aerosols. Gravitational settling of
291 aerosols between 900-600 hPa that may lead to significant amount aerosols with nitrate
292 on its surfaces through heterogeneous processes which accumulate just above the
293 inversion. At Dakar, very moist conditions (RH > 80%) are found from the surface to the
294 950 hPa just below the inversion associated with the SAL. Even though the inversion
295 inhibits vertical motions, some mixing between the SAL layer and shallow moist layer
296 below is possible.

297 Vlasenko et al. (2006) show in laboratory studies that nitrate-coated dust aerosols
298 will increase their hygroscopicity in the presence of high relative humidity. Twohy et al.
299 (2009) and Ismail et al. (2010) show that some SAL events have areas of enhanced
300 moisture embedded within the SAL and that dust particles from the desert have
301 hydroscopic properties and can serve as cloud condensation nuclei (CCN). A critical
302 threshold of moisture on the surface of the aerosols could lead water stressed microbes to
303 denitrify and release airborne biogenic NO_X leading to higher O_3 concentrations.

304 Other findings reported also include:

- Elevated O_3 concentrations on 12 June are likely caused by a stratospheric intrusion based on WRF-CHEM results and potentially enhanced NO_X emissions from dry Sahelian soils with the passage of an AEW. However, lightning-NO_X leading to O_3 enhancement followed by downward vertical transport by convective downdrafts cannot be ruled out as an additional source for 12 June (Jenkins et al. 2008b; Grant et al. 2008).
- During the transition between the pre-monsoon and monsoon periods (26 June and 2 July) a significant enhancement of O_3 concentrations in the lower/middle troposphere are found after precipitation events in area surrounding Dakar on 28 June and 1 July 2008. We suggest that pulses of biogenic NO_X emissions from dry Sahelian soils are the primary cause of enhanced O_3 concentrations consistent with early studies (Stewart et al. 2008; Delon et al. 2008; Delon et al. 2010).
- Low O_3 concentrations are found in the 925-550 hPa layers during the monsoon period (27 August and 3 September) and likely linked to dry deposition of O_3 and dry/wet deposition NO_X and HNO_3 during the monsoon period (Grant et al. 2008; Delon et al. 2010).

Additional chemical, radiative and aerosol measurements along with chemical modeling on a regional basis in West Africa will provide additional insights into the processes that control O_3 concentrations in the lower troposphere.

Acknowledgements

326 This work was supported by ATM-0621529. We thank all of the Met operators for their
327 help in this project. We thank Didlier Tanre for their efforts in establishing and
328 maintaining the Mbour, Senegal site.

329

References

Berg, R.: Tropical Cyclone Report Hurricane Ike (AL092008), National Hurricane Center http://www.nhc.noaa.gov/2008atlan.shtml, 2008.

Bian, H. and Zender C. S.: Mineral dust and global tropospheric chemistry: Relative roles of photolysis and heterogeneous uptake, J. Geophys. Res., 108, 4672, doi:10.1029/2002JD003143, 2003.

Bonasoni, P. et al.: Aerosol-ozone correlations during dust transport episodes, Atmos. Chem. Phys. 4, 1201-1215, 2004.

Burpee, R. W.: The Origin and Structure of Easterly Waves in the Lower Troposphere of North Africa, J. Atmos. Sci., 29, 77-90, 1972.

Camara, M., Jenkins, G. S., Konare, A.: Impact of dust on West African Climate during 2005 and 2006, Atmos. Chem. Phys., 10, 3053-3086, 2010.

Carlson T. and Prospero, J. M.: The Large-Scale Movement of Saharan Air Outbreaks over the Northern Equatorial Atlantic, J. Appl. Meteorol., 11, 283-297, 1972.

De Reus, M. et al.: Airborne observations of dust aerosols over the North Atlantic during ACE2: Indications for heterogeneous ozone destruction, J. Geophys. Res., 105, 15-263-15,275, 2000.

Delon, C., Reeves, C. E., Stewart, D. J., Serça, D., Dupont, R., Mari, C., Chaboureau, J.-P., and Tulet, P.: Biogenic nitrogen oxide emissions from soils – impact on NO_x and ozone over West Africa during AMMA (African Monsoon Multidisciplinary Experiment): modelling study, Atmos. Chem. Phys., 8, 2351-2363, 2008.

Delon, C., et al.: Atmospheric nitrogen budget in Sahelian dry savannas, Atmos. Chem. Phys., 10, 2691-2708, 2010.

Dunion, J. P., and Velden C. S.: The impact of the Saharan air layer on Atlantic tropical cyclone activity, B. Am. Meteorol. Soc., 85, 353–365, doi:10.1175/BAMS-85-3-353, 2004.

Fast, J., et al.: Evolution of ozone, particulates, and aerosol direct radiative forcing in the vicinity of Houston using a fully coupled meteorology-chemistry-aerosol model, J. Geophys. Res., 111, D21305, doi:10.1029/2005JD006721, 2006.

Grant et al.: Ozone Transport by Mesoscale Convective Systems in Western Senegal, Atmos. Environ., 42, 7104–7114, 2008.

Grell, G. A., et al.: Fully coupled "online" chemistry within the WRF model, Atmos. Environ., 39, 6957–6975, 2005.

Guenther, A. et al: A global model of natural volatile organic compound emissions, J J. Geophys. Res., 100, 8873-8892, 1995.

Ismail, S. et al.: LASE Measurements of Water Vapor, Aerosols and Cloud Distributions in Saharan Air Layers and Tropical Disturbances, J. Atmos. Sci., 67, 1026-1047, 2010.

Jacob, D. J.: Heterogeneous chemistry and tropospheric ozone, Atmos. Environ., 24, 2131-2159, 2000.

Jaeglé, L et al.: Satellite mapping of rain-induced nitric oxide emissions from soils, J. Geophys. Res., 109, D21310, doi:10.1029/2004JD004787, 2004.

373 Jenkins, G.S., Pratt, A. Heymsfield, A. Possible linkages between Saharan dust and
374 Tropical Cyclone Rain Band Invigoration in Eastern Atlantic during NAMMA-
375 06, Geophys. Res. Lett., doi:10.1029/2008GL034072, 2008.

376 Jenkins, G. S., Camara, M., Ndiaye, S.: Observational Evidence of enhanced
377 middle/upper tropospheric ozone via convective processes over the Equatorial
378 Tropical Atlantic during the summer of 2006, Geophys. Res. Lett., 35,
379 doi:10.1029/2008GL033954, 2008b.

380 Middleton, N. J. and A. S. Goudie, A. S.: Saharan dust: Sources and trajectories, T. I.,
381 Brit. Geogr., 26, 165-181, 2001.

382 Myhre, G. A. et al.: Modeling the radiative impact of mineral dust during the Saharan
383 Dust Experiment (SHADE) campaign, J. Geophys. Res., 108, 8579,
384 doi:10.1029/2002JD002566, 2003.

385 Redelsperger, J. L., Thorncroft, C. D., Diedhiou, A. Lebel, T., Parker, D. J., Polcher, J.:
386 African Monsoon Multidisciplinary Analysis: An International Research Project
387 and Field Campaign, B. Am. Meteorol. Soc., 87, 1739–1746, 2006.
388 Rhome, J. R.:Tropical Cyclone Report Hurricane Bertha (AL022008), National
389 Hurricane Center http://www.nhc.noaa.gov/2008atlan.shtml, 2008.
390
391 Saunois, M. et al.: Factors controlling the distribution of ozone in the West African lower
392 troposphere during AMMA (African Monsoon Multidisciplinary Analysis) wet
393 season campaign, Atmos. Chem. Phys., 9, 6135–6155, 2009.

394 Stewart, D. J., Taylor, C. M., Reeves, C. E., and McQuaid, J. B: Biogenic nitrogen oxide
395 emissions from soils: impact on NO_x and ozone over west Africa during AMMA
396 (African Monsoon Multidisciplinary Analysis): observational study, Atmos.
397 Chem. Phys., 8, 2285-2297, 2008.
398 Tang et al.: Impacts of dust on regional tropospheric chemistry during the ACE-Asia
399 experiment: A model study with observations, J. Geophys. Res., 109,
400 doi:10.1029/2003JD003806, 2004.
401
402 Twohy, C. H., et al.: Saharan dust particles nucleate droplets in eastern Atlantic clouds,
403 Geophys. Res. Lett., 36, L01807, doi:10.1029/2008GL035846, 2009.

404 van der A. et al.: Trends, seasonal variability and dominant NO_x source derived from a
405 ten year record of NO_2 measured from space, J. Geophys. Res., 113, ,
406 doi:10.1029/2007JD009021, 2008.

407 Vlasenko, A. et al.: Effect of humidity on nitric acid uptake to mineral dust aerosol
408 particles, Atmos. Chem. Phys., 6, 2147-2160, 2006.

409 Williams, J. E et al.: The influence of biogenic emissions from Africa on tropical
410 tropospheric ozone during 2006: a global modeling study, Atmos. Chem. Phys., 9,
411 5729-5749, 2009.

412 Zhang, Y., Sunwoo, Y., Kotamarthi, V., Carmichael, G. R.: Photochemical Oxidant
413 Processes in the Presence of Dust: An Evaluation of the Impact of Dust on
414 Particulate Nitrate and Ozone Formation, J. Appl. Meteorol., 33,813-824, 1994.

415 Ziemke, J. R. et al.: Tropospheric ozone determined from Aura OMI and MLS:
416 Evaluation of measurements and comparison with the Global Modeling
417 Initiative's Chemical Transport Model", J. Geophys. Res., 111,
418 doi:10.1029/2006JD007089, 2006.
419
420
421 Zipser, E.J. et al.: The Saharan Air Layer and the Fate of African Easterly Waves—
422 NASA's AMMA Field Study of Tropical Cyclogenesis, B. Am. Meteorol. Soc., 90,
423 1137–1156, 2009.
424
425
426
427 **Figure Captions**

428 **Figure 1.** OMI/MLS Total Column Ozone for (a) June 2008; (b) July 2008; (c) August
429 2008; (d) September 2008. Units are in DU.

430 **Figure 2.** Daily area averaged (13-16°N, 16-19°W) OMI derived Aerosol Index (AI) and
431 Mbour, Senegal AOT for:(a) June; (b) July; (c) 1 August-5 September; (d) Area averaged
432 (11.5-16.5°N, 12.5-17.5°W) TRMM daily averaged precipitation for 1 June-5 September
433 2006.

434 **Figure 3.** 1000-450 hPa lower/middle tropospheric vertical profiles of O_3 concentrations
435 for: (a) all launches; (b) 26 June and 2 July. Units are ppb.

Figure 4. 1000-450 hPa lower/middle tropospheric vertical profiles of: (a) O_3 concentrations; (b) relative humidity and (c) temperature for the pre-monsoon period.

Figure 5. Pre-Monsoon OMI AI/925 hPa streamlines and Deep Blue AOT/700 hPa streamlines: (a, f) 8 June; (b, g); 10 June; (c, h) 12 June; (d, i) 15 June; (e, j) June 26.

Figure 6. TRMM daily Precipitation amounts (a) 28 June; (b) 29 June; (c) 30 June; (d) 1 July. Units are mm.

Figure 7. 1000-450 hPa lower/middle tropospheric vertical profiles of: (a) O_3 concentrations; (b) relative humidity and (c) temperature for the monsoon period.

Figure 8. Monsoon OMI AI/925 hPa streamlines and Deep Blue AOT/700 hPa streamlines: (a, e) 2 July; (b, f); 2 August; (c, g) 27 August; (d, h) 3 September.

Figure 9. Time-height profiles of O_3 concentrations and vertical velocity at 14.5° N, 17.5°W for initial conditions beginning at: (a) 1 June 0000 UTC; (b) 4 June 1200 UTC; (c) 5 June 1200 UTC; (d) 6 June 1200. Units in ppb and cm-s^{-1}.

Figure 10. 1000-150 hPa vertical profile of O_3 at Dakar for 10,12 June, 1200 UTC. Units in ppb.

Figure 11. WRF-Chem simulation of: (a) 925 hPa O_3 concentrations for June, July and August; (b) 850 hPa relative humidity for June, July and August.

Figure 12. 1000-750 hPa vertical profiles of O3 (blue), RH (green) and Temperature (red) for identified SAL events. (a) 8 June; (b) 10 June; (c) 15 June; (d) 2 August. Units are ppb for O_3, % for RH and Degree C for temperature.

Figure 13. (a) A depiction of relative humidity, aerosol and O_3 concentrations in various layer of the lower/middle troposphere associated with a SAL intrusion. The dash line represents the vertical profile of temperature. (b) Proposed mechanism for increasing O_3 in the 950-900 hPa layer.

Date (2008)	Time (UTC)	O_3 925-550 hPa (DU)	RH 925-550 hPa (%)	OMI AI (13-16°N, 16-19°W)
8 June	1200	6.6	32.2	2.11
10 June	1200	7.4	37.3	1.29
12 June	1200	20.5	65.1	
15 June	1200	11.3	28.7	2.02
26 June	1200	10.5	37.2	1.98
2 July	1200	14.2	67.3	
2 August	1200	10.3	31.3	3.80
27 August	1200	6.4	88.5	0.58
3 Sept	1200	11.0	68.8	0.61

Table 1: Surface -550 hPa Column O_3, Relative humidity and OMI AI index.

476

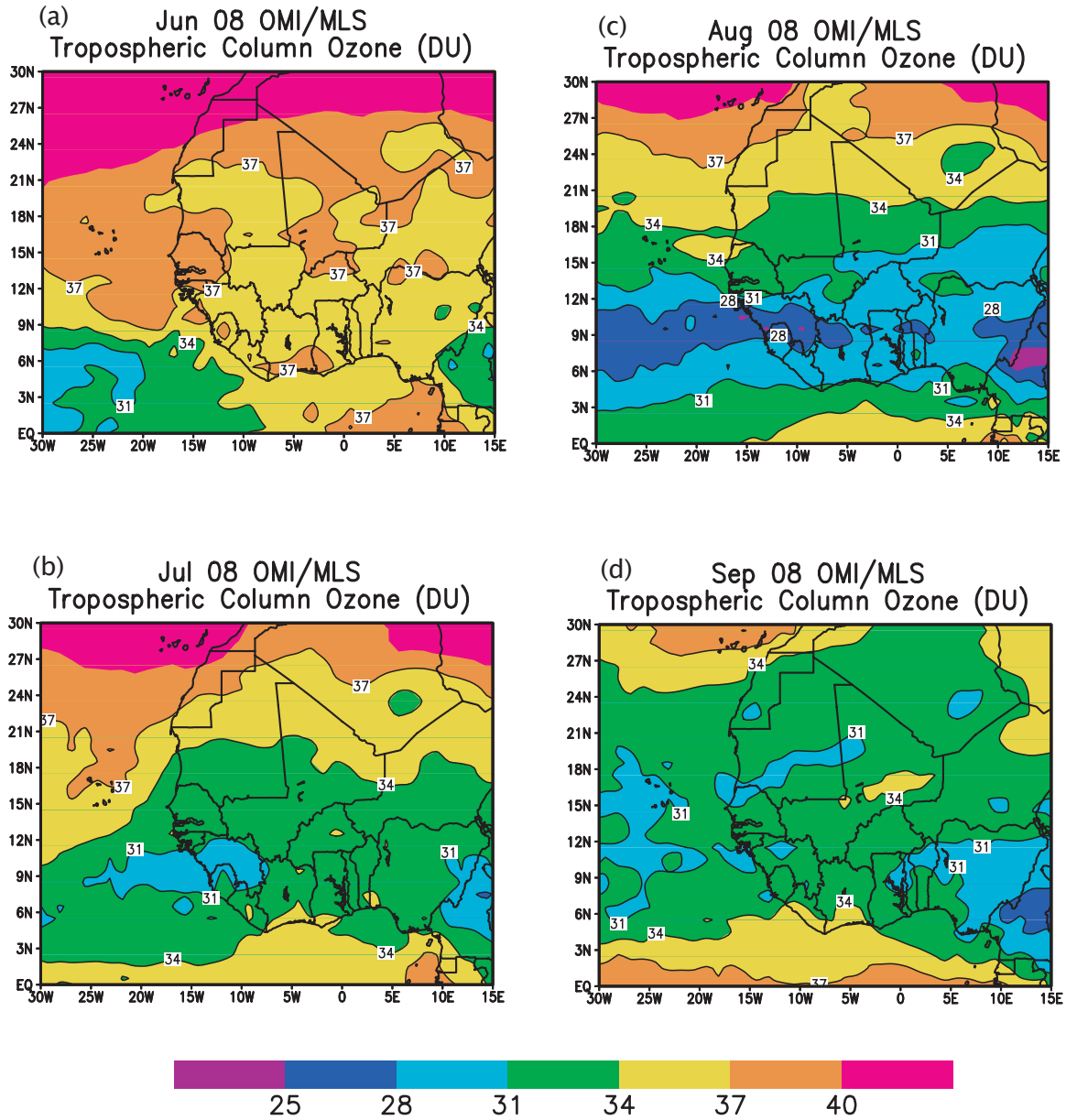

477
478

479 **Figure 1.** OMI/MLS Total Column Ozone for (a) June 2008; (b) July 2008; (c) August
480 2008; (d) September 2008. Units are in DU.

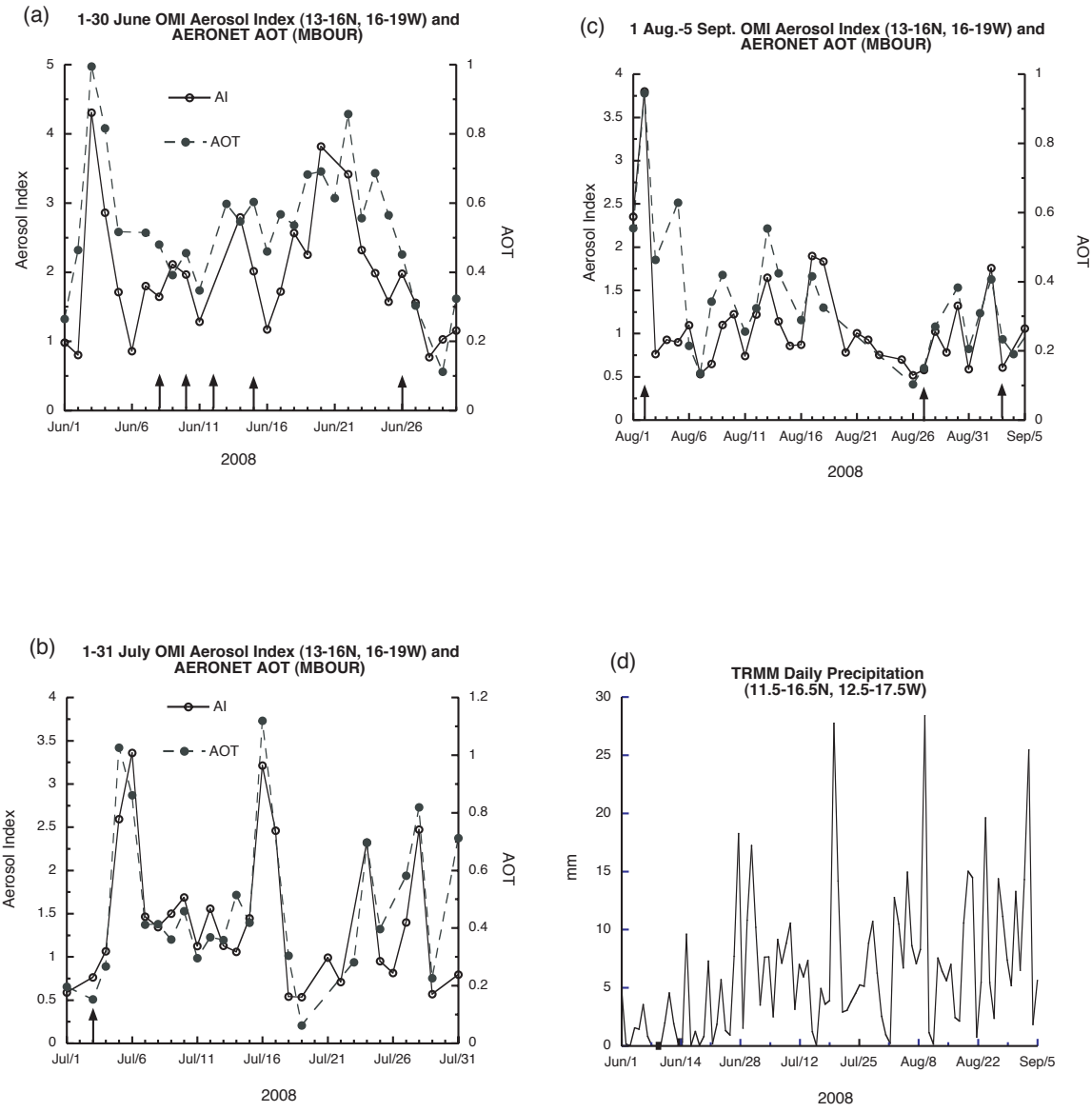

Figure 2. Daily area averaged (13-16°N, 16-19°W) OMI derived Aerosol Index (AI) and Mbour, Senegal AOT for:(a) June; (b) July; (c) 1 August-5 September; (d) Area averaged (11.5-16.5°N, 12.5-17.5°W) TRMM daily averaged precipitation for 1 June-5 September 2006.

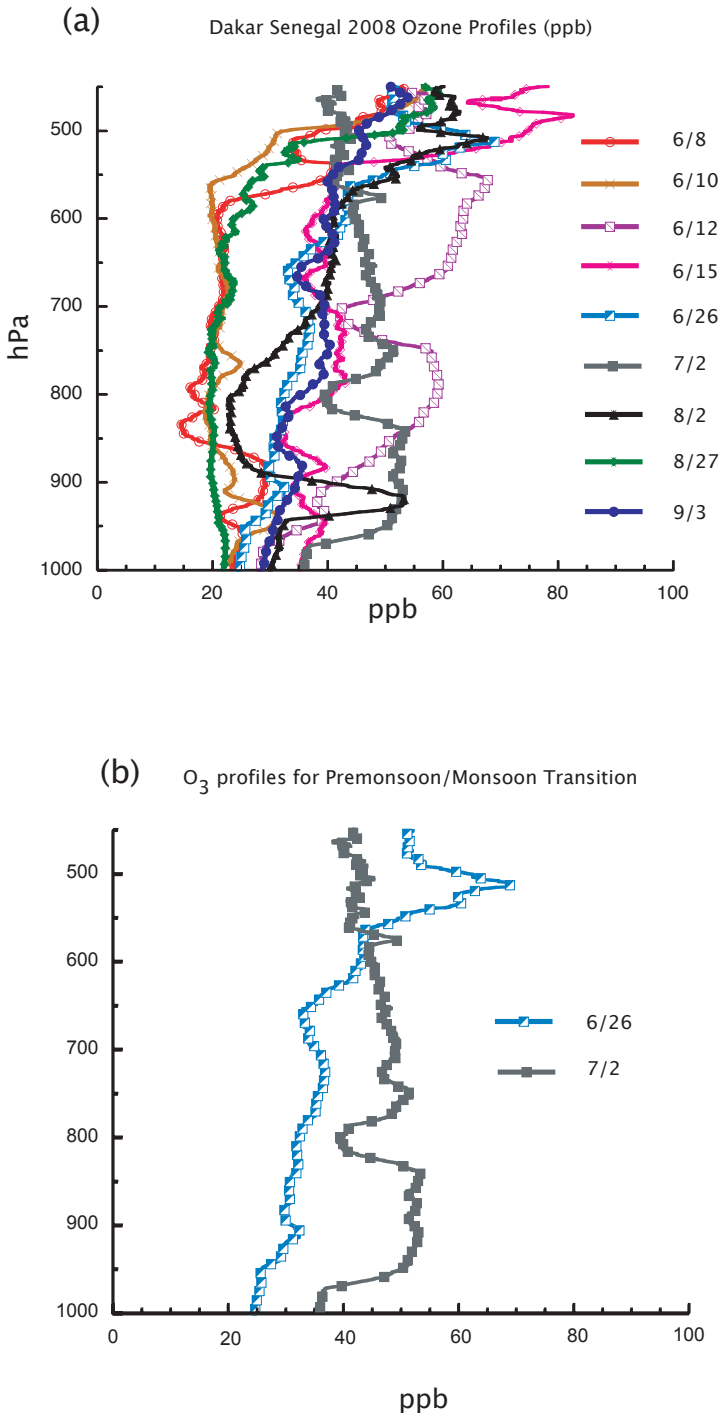

488

489 **Figure 3.** 1000-450 hPa lower/middle tropospheric vertical profiles of O_3 for: (a) all

490 launches; (b) pre-monsoon period and; (c) monsoon periods; (d) 26 June and 2 July.

491 Units are ppb.

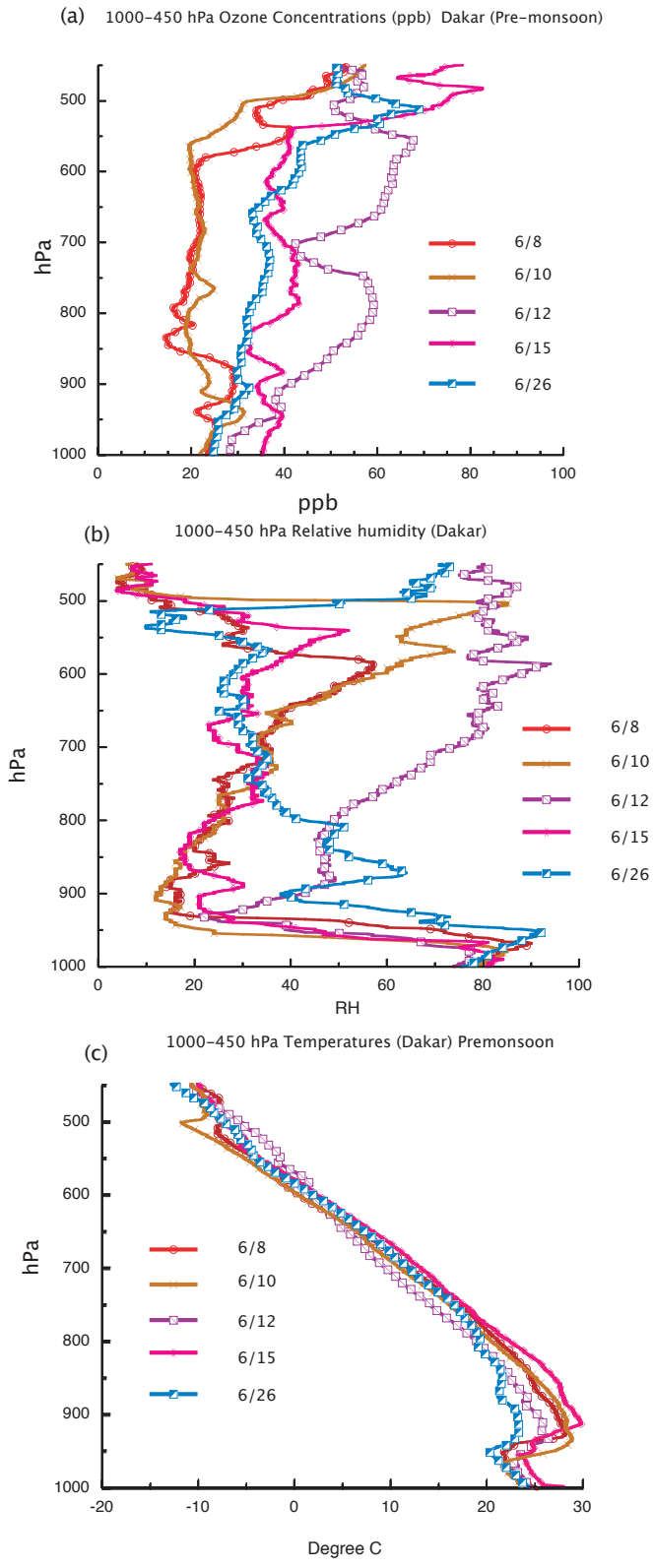

Figure 4. 1000-450 hPa lower/middle tropospheric vertical profiles of: (a) O_3 concentrations; (b) relative humidity and (c) temperature for the pre-monsoon period.

(a) June 8 OMI AI /925 hPa Streamlines

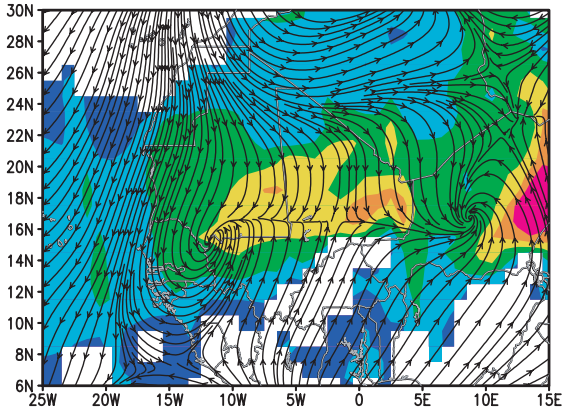

(f) June 8 Deep Blue (AOD)/700 hPa Streamlines

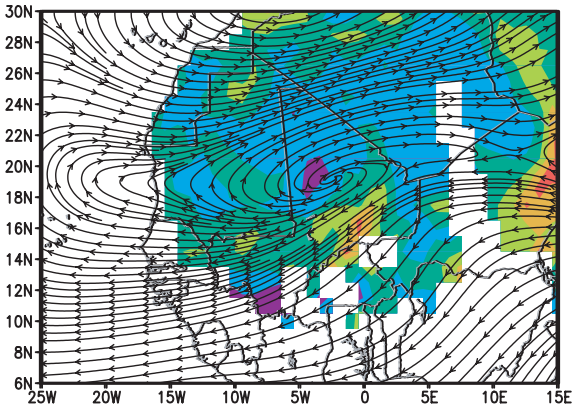

(b) June 10 OMI AI /925 hPa Streamlines

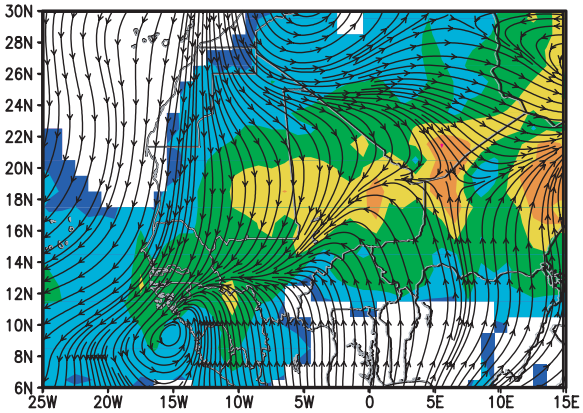

(g) June 10 Deep Blue (AOD)/700 hPa Streamlines

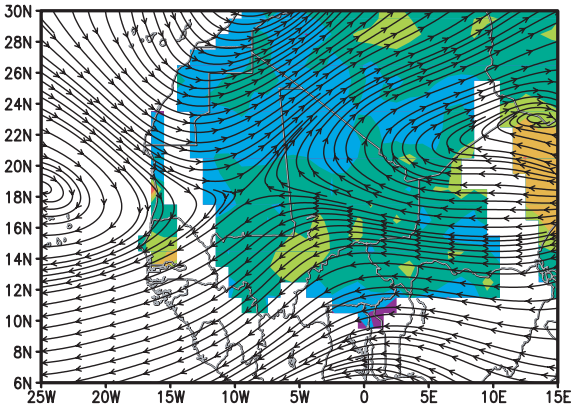

(c) June 12 OMI AI /925 hPa Streamlines

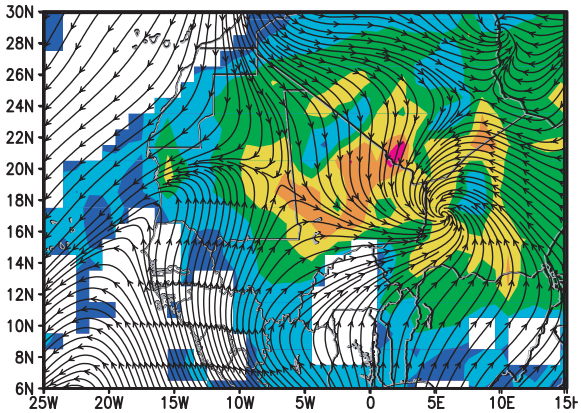

(h) June 12 Deep Blue (AOD)/700 hPa Streamlines

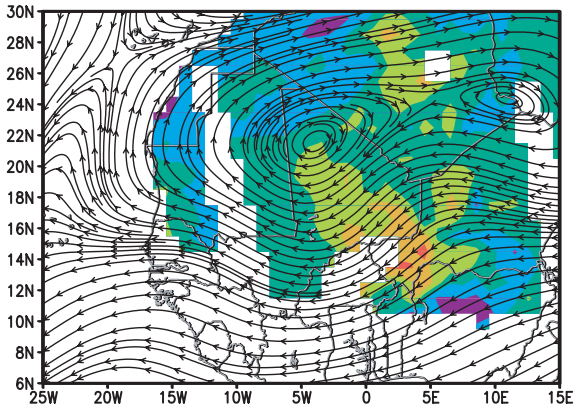

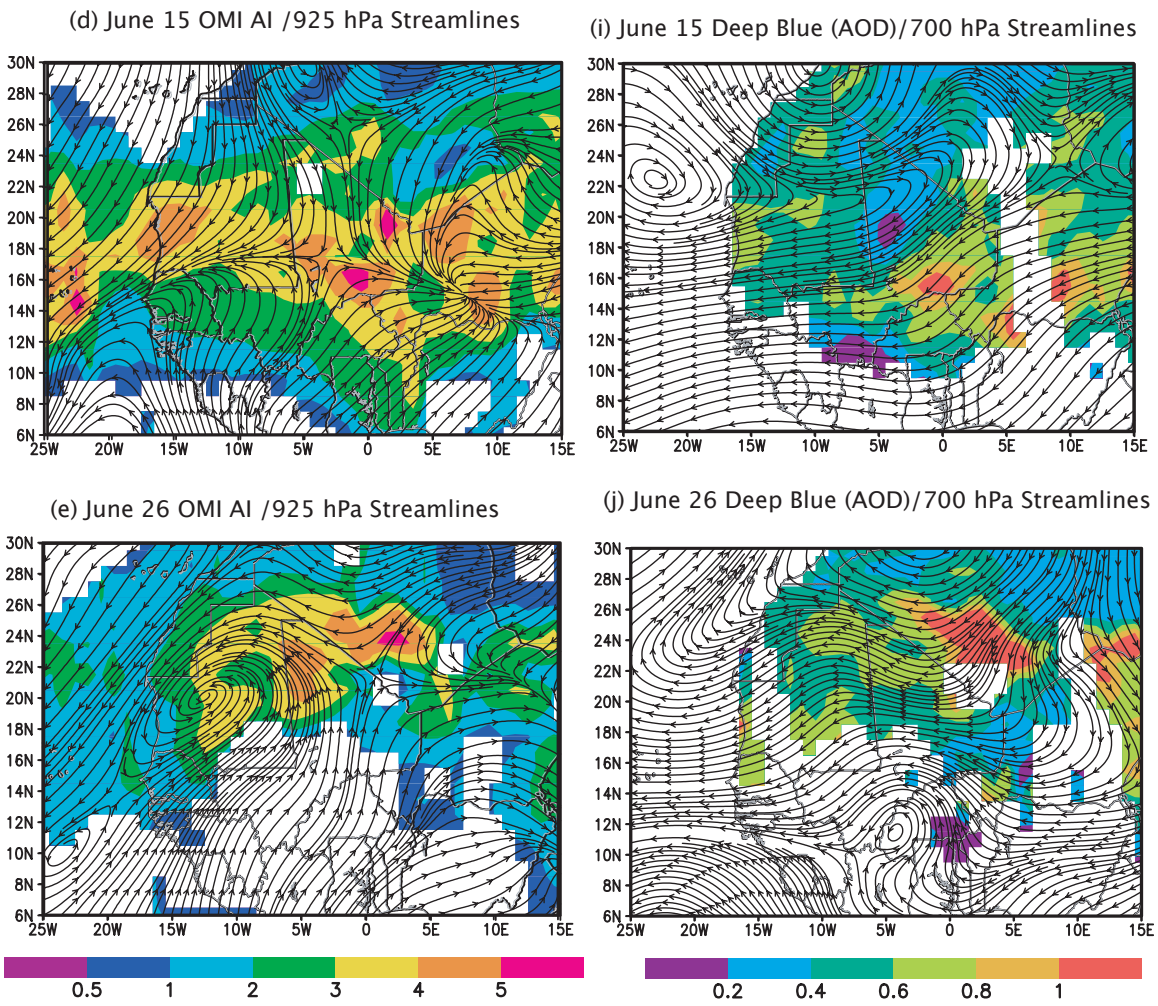

496

497 **Figure 5.** Pre-Monsoon OMI AI/925 hPa streamlines and Deep Blue AOT/700 hPa

498 streamlines: (a, f) 8 June; (b, g); 10 June; (c, h) 12 June; (d, i) 15 June; (e, j) June 26.

499

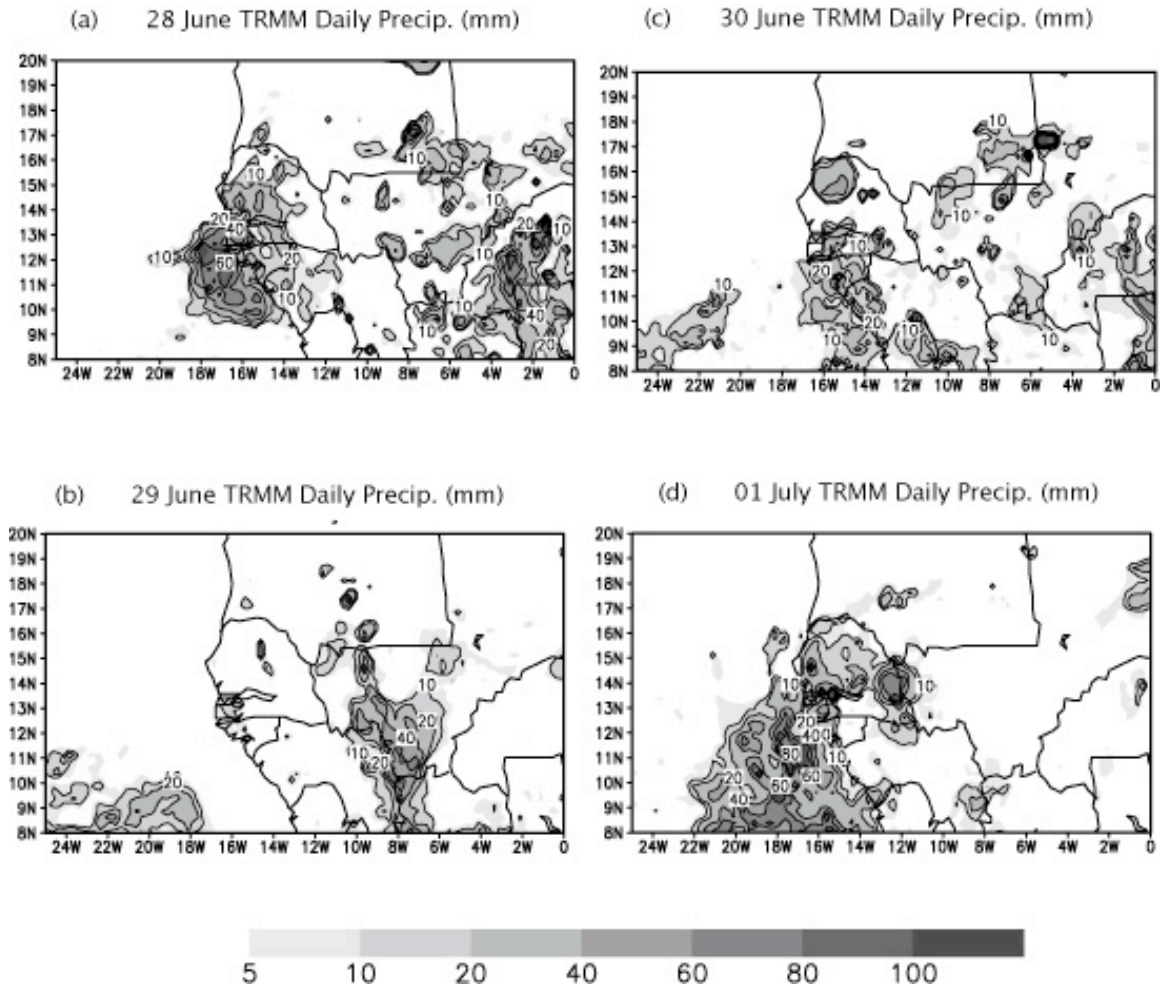

500

501

502 **Figure 6**. TRMM daily Precipitation amounts (a) 28 June; (b) 29 June; (c) 30 June; (d) 1
503 July. Units are mm.

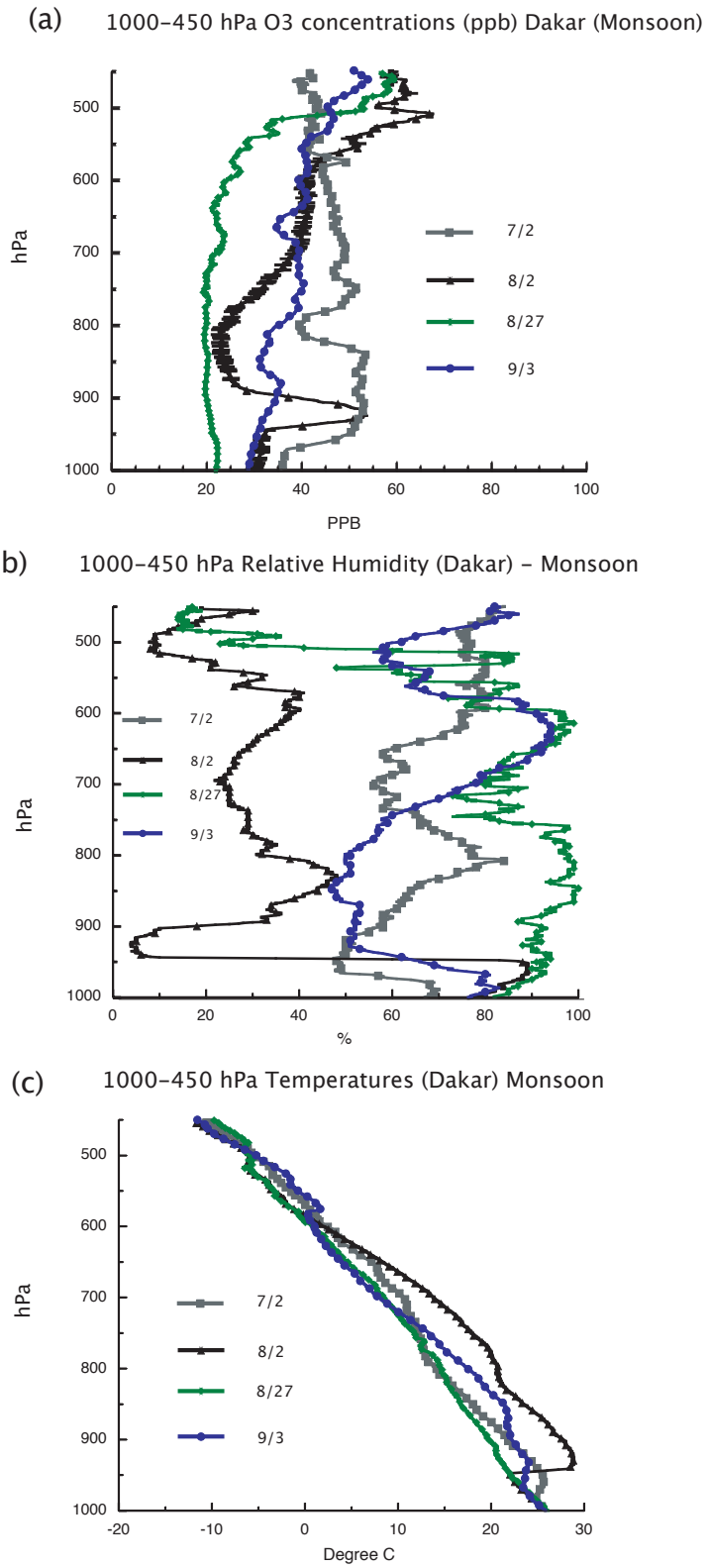

Figure 7. 1000-450 hPa lower/middle tropospheric vertical profiles of: (a) O_3 concentrations; (b) relative humidity and (c) temperature for the monsoon period

(a) 02 July OMI AI /925 hPa Streamlines

(e) 02 July Deep Blue (AOD)/700 hPa Streamlines

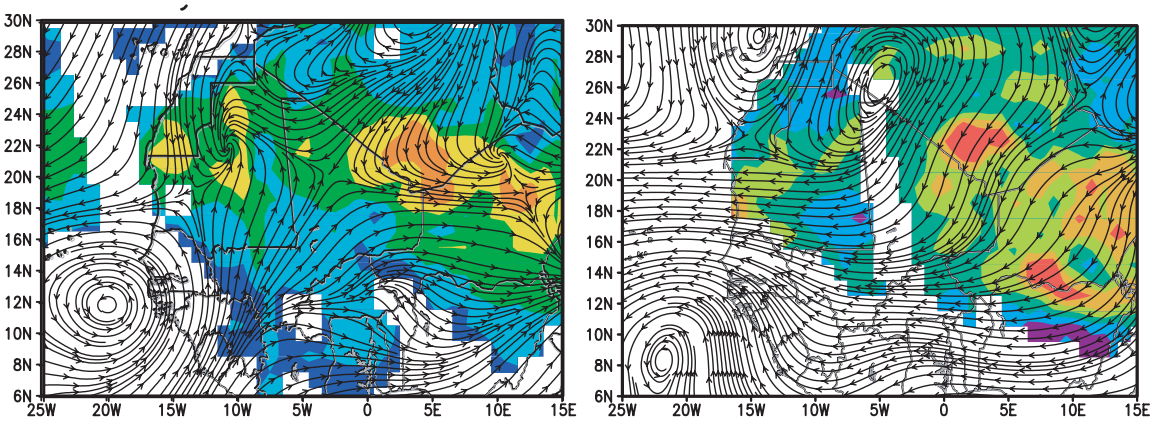

(b) 02 Aug. OMI AI /925 hPa Streamlines

(f) 02 Aug. Deep Blue (AOD)/700 hPa Streamlines

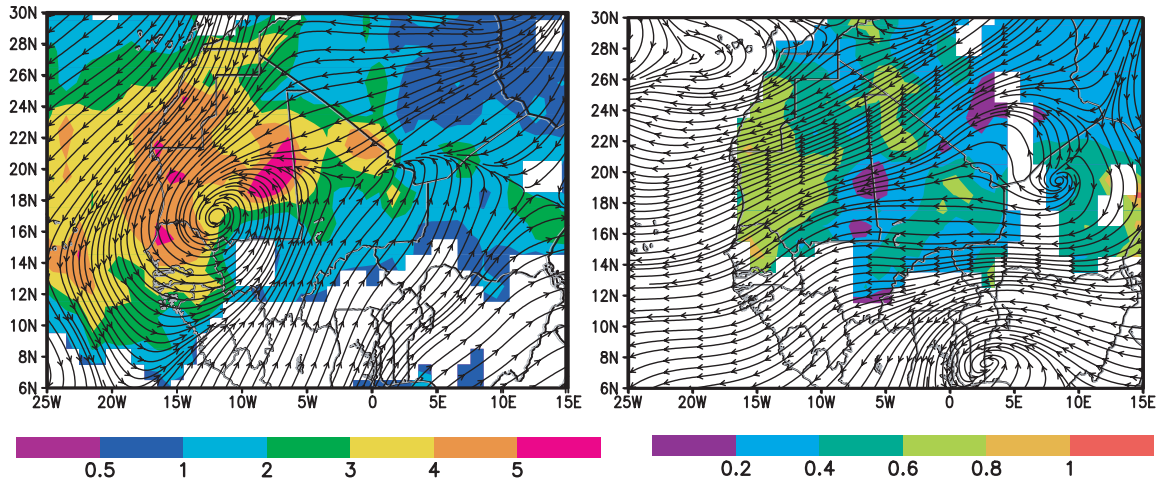

507

508

509

510

511

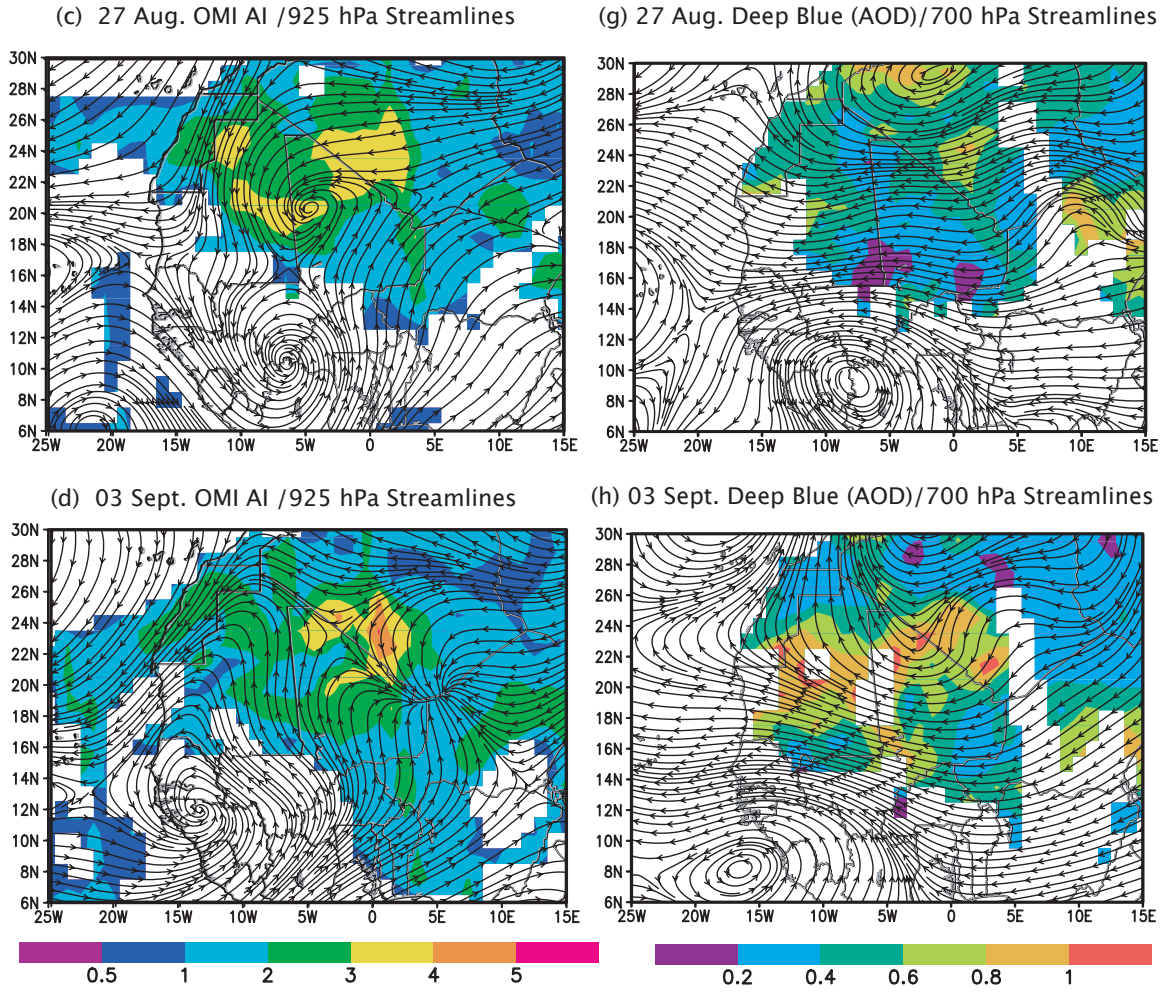

512

513

514 **Figure 8.** Monsoon OMI AI/925 hPa streamlines and Deep Blue AOT/700 hPa

515 streamlines: (a, e) 2 July; (b, f); 2 August; (c, g) 27 August; (d, h) 3 September.

516

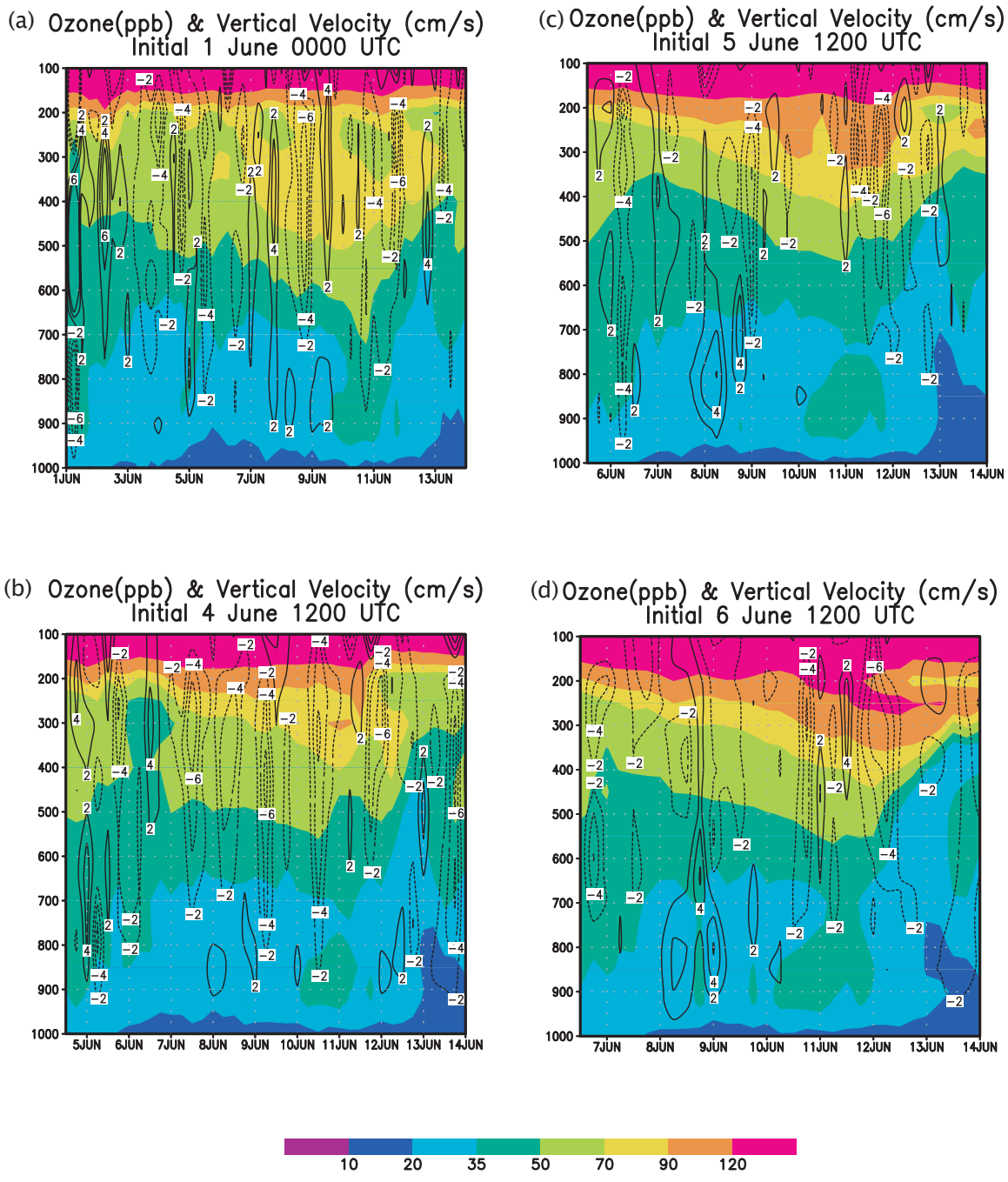

Figure 9. Time-height profiles of O_3 concentrations and vertical velocity (w) at 14.5° N, 17.5°W for initial conditions beginning at: (a) 1 June 0000 UTC; (b) 4 June 1200 UTC; (c) 5 June 1200 UTC; (d) 6 June 1200. Units in ppb and cm-s^{-1}.

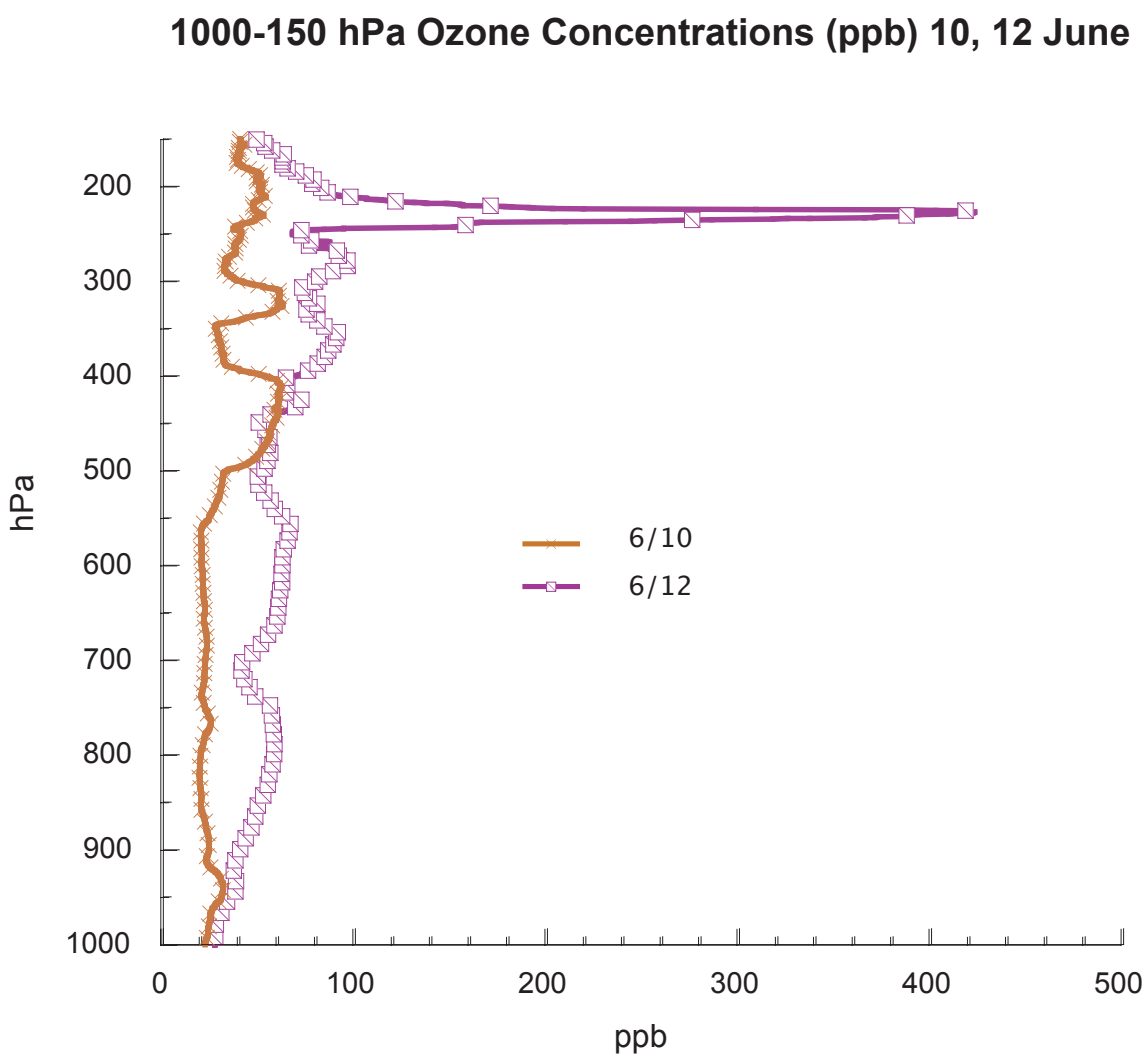

Figure 10. 1000-150 hPa vertical profile of O_3 at Dakar for 10,12 June, 1200 UTC. Units in ppb.

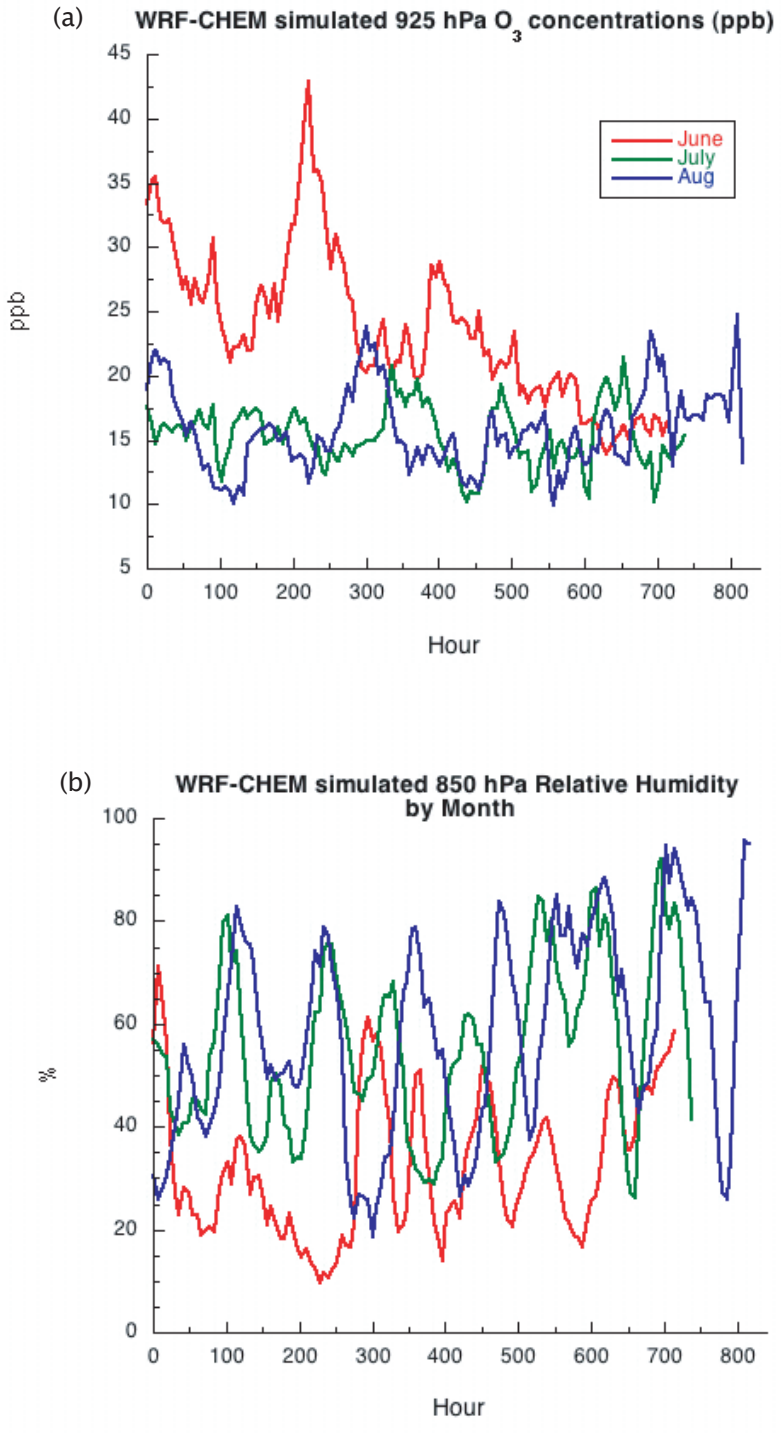

531

532 **Figure 11.** WRF-Chem simulation of: (a) 925 hPa O_3 concentrations for June, July and

533 August; (b) 850 hPa relative humidity for June, July and August.

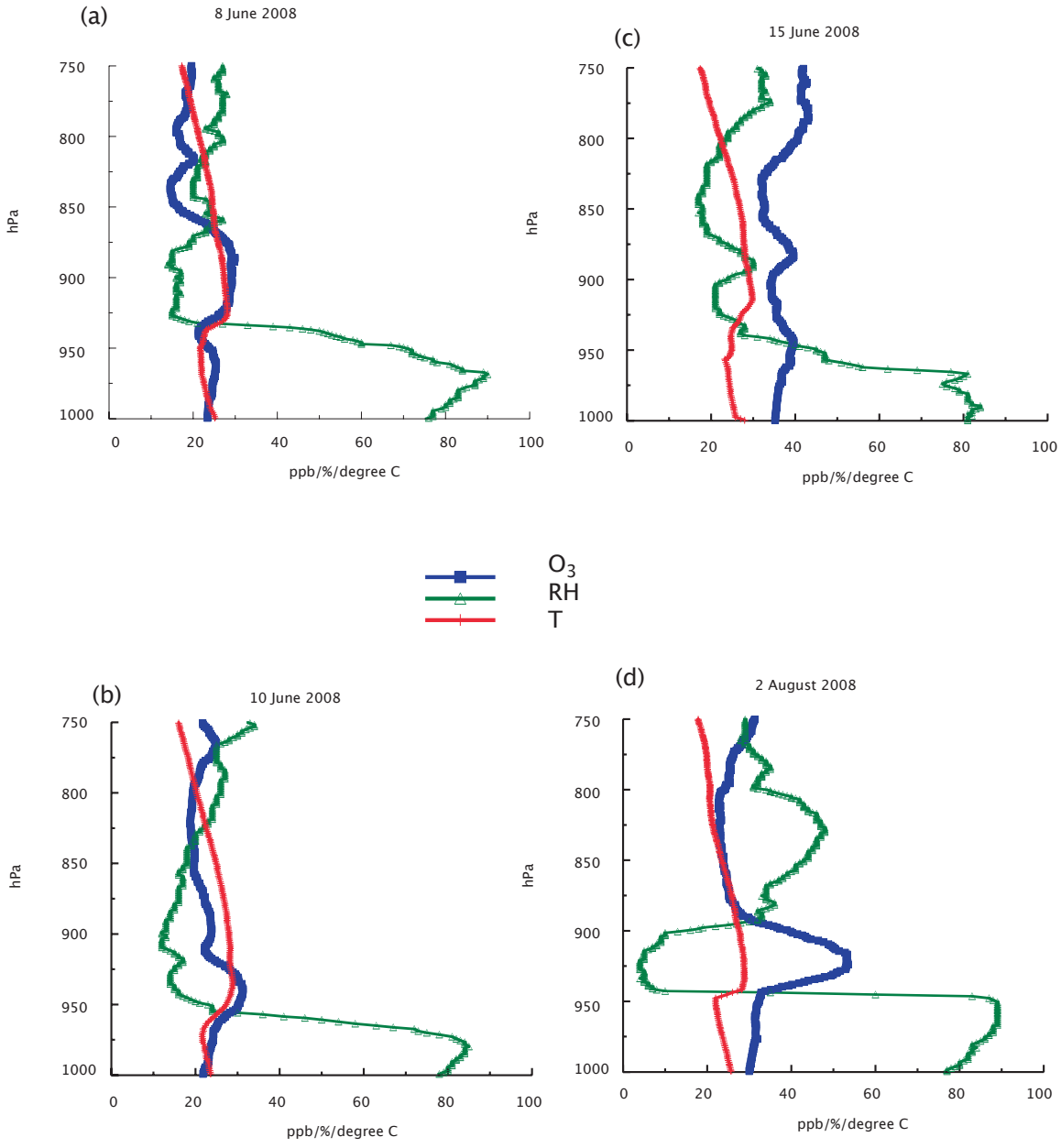

Figure 12. 1000-750 hPa vertical profiles of O3 (blue), RH (green) and Temperature (red) for identified SAL events. (a) 8 June; (b) 10 June; (c) 15 June; (d) 2 August. Units are ppb for O3, % for RH and Degree C for temperature.

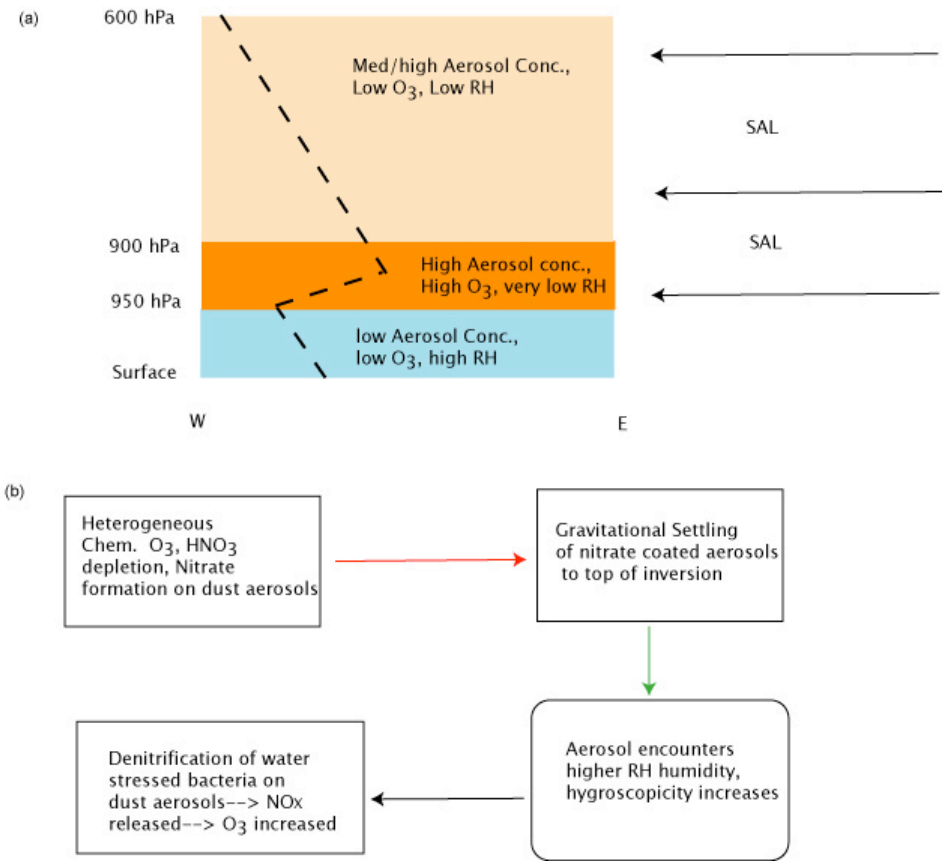

Figure 13. (a) A depiction of relative humidity, aerosol and O_3 concentrations in various layer of the lower/middle troposphere associated with a SAL intrusion. The dash line represents the vertical profile of temperature. (b) Proposed mechanism for increasing O_3 in the 950-900 hPa layer